Vietnam Journal of Mechanics, Vol. 46, No. 4 (2024), pp. 311 – 330
DOI: https://doi.org/10.15625/0866-7136/21113

ANALYTICAL MODELING AND COMPUTATIONAL OPTIMIZATION FOR A 1-DOF COMPLIANT MECHANISM

Hung Dinh Nguyen[1], Hung Van Le[2], Minh Phung Dang[2], Hieu Giang Le[2], Thanh-Phong Dao[2,*]

[1]*Faculty of Mechanical Engineering, Industrial University of Ho Chi Minh City, Ho Chi Minh City, Vietnam*

[2]*Faculty of Mechanical Engineering, Ho Chi Minh City University of Technology and Education, Ho Chi Minh City, Vietnam*

[*]E-mail: dtphong@hcmute.edu.vn

Received: 09 July 2024 / Revised: 19 September 2024 / Accepted: 02 October 2024
Published online: 24 October 2024

Abstract. The first natural frequency directly affects the operational conditions of compliant mechanisms in precision engineering systems. To address this challenge, a computational method based on the surface response method is proposed to optimize the frequency of a new one degree of freedom (DOF) compliant mechanism. Initially, a 1-DOF 3D model of a compliant mechanism is built. The dynamic equation and the frequency response are formulated via equivalent stiffness and the Lagrange method. Subsequently, a series of numerical simulations are conducted to find the fundamental frequency of the mechanism. The initial dimensions of the flexible joints are determined, and the initial frequency is analyzed by using finite element analysis. Next, the flexible joints in the designed mechanism are optimized by a variant of the genetic algorithm. The optimized dimensions of the mechanism are found with the thickness of the circular joint of 1.10 mm, the thickness of the leaf joint of 1.19 mm, and the length of the leaf joint of 54.50 mm. The optimized result showed that there is a significant improvement in the frequency of the mechanism, increasing from an initial design of 53.218 Hz to an optimal design of 75.927 Hz with an improvement of 42.6%. This study provides important reference materials for future research on compliant mechanisms.

Keywords: 1-DOF compliant mechanism, equivalent stiffness, dynamic modeling, Lagrange method, finite element analysis.

1. INTRODUCTION

Compliant mechanisms have been widely applied in various fields, including medicine [1, 2], MEMS [3, 4], and precision engineering [5]. Due to their advantages of simple structure, precise motion, and minimal energy loss attributed to the compliant nature of their motion model, compliant mechanisms play a crucial role in devices, directly influencing their performance and accuracy. Operating at high speeds poses challenges in ensuring rapid response of internal components and raises issues regarding the optimal frequency of the mechanism. While previous studies on compliant mechanisms have addressed some limitations, such as suboptimal structures and inadequate consideration of natural frequencies, resulting in predominantly low resonance frequencies [6] and consequent slow response during operation [7]. Up to now, many analytical methods have been developed (e.g., pseudo-rigid-body model, compliance matrix, etc.) for analyzing the characteristics of compliant mechanisms but they are still limited for large behaviors [6, 8]. According to the literature review, the first natural frequency is an important response of a structure. When a dynamic equation, it is known that the frequency is directly related to the dynamic response. When the frequency is high or low, it can avoid the resonant phenomenon as well as enhance the speed of the system. Hence, this paper also considers the frequency in the design phase.

The one degree of freedom (DOF) compliant mechanism is a monolithic structure which is designed for wide applications in precise positioning systems. It can provide a smooth motion from a few micrometers to hundreds of micrometers. The designed mechanism can be applied for micro/nano-indentation, vibration-assisted machining, alignment, precise positioner, and so on. In this study, based on practical insights from mechanical devices and on design and fabrication experience, this article regards the first frequency to avoid the resonant phenomenon for the mechanism as well as enhance the dynamic response. To effectively address these issues, this paper proposes a numerical approach based on finite element analysis to achieve a best solution for a final design of 1-DOF compliant mechanism.

The purpose of this paper is to provide a visual analysis that facilitates the modeling and analysis of the 1-DOF compliant mechanism. The dynamic equation of the designed mechanism has been developed via equivalent stiffness and the Lagrange method to determine the initial frequency of the mechanism before optimization. Subsequently, a series of FEA simulations were conducted to compare errors and validate the accuracy between the two methods. In this study, the 1-DOF mechanism is optimized through the use of the water cycle algorithm, resulting in an increased frequency of the mechanism that meets the design objectives after optimization. The optimal solution is then numerically verified.

2. MECHANISM DESIGN

2.1. Module design of 1-DOF compliant mechanism

The 1-DOF mechanism is potentially used for precise positioning system in terms of quick dynamic response. In this part, the mechanical design scheme of the 1-DOF mechanism is shown in Fig. 1. The suggested mechanism consists of a lever-type amplification mechanism and various types of joints, including right circular joints and leaf joints, as illustrated in Fig. 2. The designed mechanism has overall dimensions of 271.82 $\times$ 194.21 $\times$ 10 mm^3, with the dimensions and weights of the components detailed in Tables 1 and 2. The mechanism is desired to be manufactured using 3D printing; therefore, the polylactic acid (PLA) is chosen and its properties are provided in Table 3.

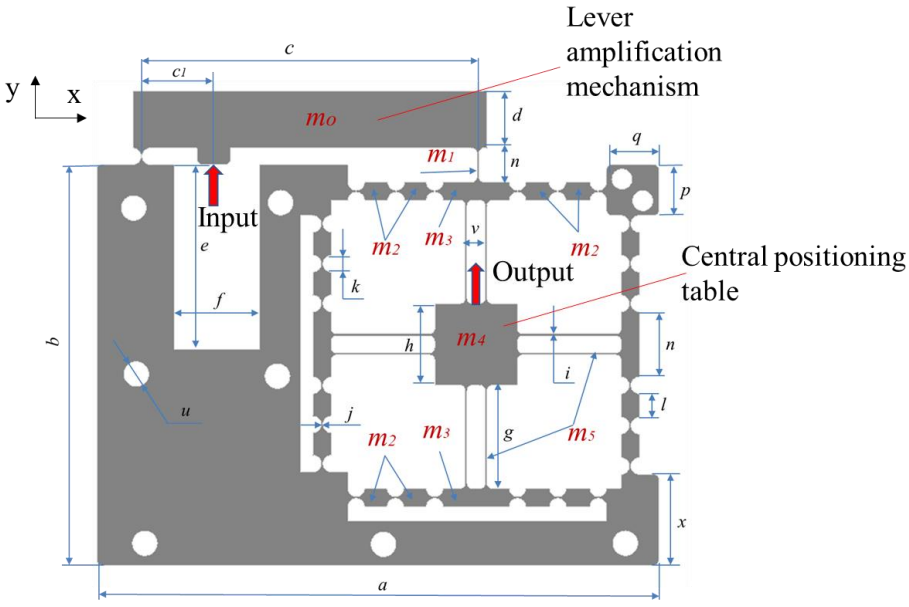

Fig. 1. Full design diagram of the 1-DOF compliance mechanism

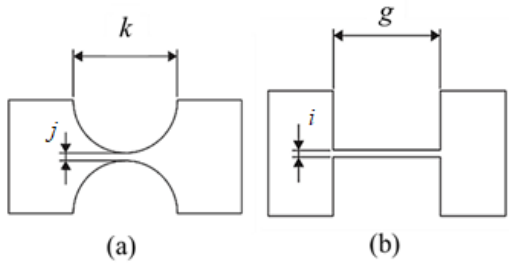

Fig. 2. Common flexure hinges: (a) right circular hinge, (b) leaf hinge

Table 1. The dimensional parameters of the 1-DOF compliant mechanism

Symbol	Value	Unit	Symbol	Value	Unit
a	271.82	mm	k	8.02	mm
b	194.21	mm	l	10.94	mm
c	160.9	mm	m	31.65	mm
d	27.66	mm	n	16.52	mm
e	89.66	mm	p	24.71	mm
f	41.19	mm	q	25.26	mm
g	50	mm	u	12	mm
h	39.68	mm	c_1	43.51	mm
i	0.9	mm	v	8.73	mm
j	0.8	mm	x	44.04	mm

Table 2. The mass values of links

Symbol	Value	Unit
m_0	0.059	kg
m_1	0.000 186	kg
m_2	0.0012	kg
m_3	0.003 49	kg
m_4	0.0197	kg
m_5	0.000 56	kg

Table 3. PLA plastic material [9,10]

Young modulus (GPa)	Poisson's Ratio	Yield strength (MPa)	Ultimate tensile strength (MPa)	Density (kg/m^3)	Melting point ($^\circ$C)
3.5	0.4	72	26.4	1250	145-177

The degrees of freedom of the mechanism are determined based on the movement direction of the central positioning table. In this design, an input displacement is exerted to the amplifier, it causes the central positioning table to move only up and down in one direction, specifically along the Y-axis. Therefore, the degrees of freedom in the mechanism are determined to be 1. The designed mechanism is desired to achieve a high dynamic response to avoid a resonant phenomenon and speed up the positioning ability.

2.2. Kinematic scheme and working principle of the 1-DOF module

The 1-DOF mechanism is moved along the Y-axis with an input actuation from the lever amplifier, and m will be moved and create an angle φ_0, as shown in Fig. 3. In this case, the mechanism includes kinetic and potential energy. The potential energy of the mechanism while in motion includes the elastic energy stored in the right circular joints and leaf joints, which are assumed to be springs. The equivalent spring system consists of the springs of these joints which are arranged in parallel and in series, as shown in Fig. 4.

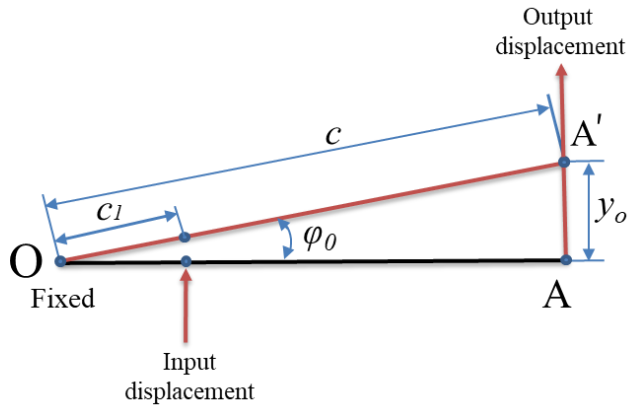

Fig. 3. Working principle and corresponding amplification ratio of lever amplifier

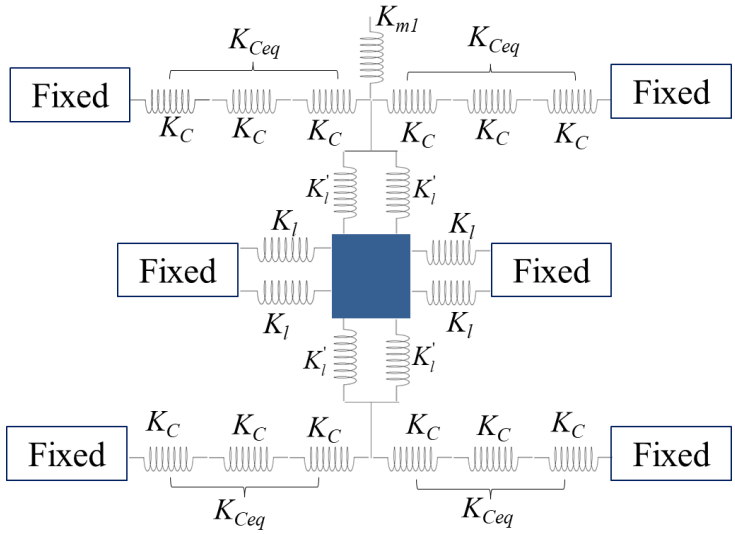

Fig. 4. Schematic representation of the springs for the joints in the mechanism

3. ANALYTICAL MODELING

3.1. Dynamic analysis

The stiffness K_c of a right circular joint is determined in the case of bending stiffness by

$$K_c = \frac{2Ebj^{2.5}}{9\pi\left(\frac{k}{2}\right)^{0.5}}.$$

The stiffness K_l of the leaf joint is calculated when bending hardness occurs as

$$K_l = \frac{Ei^3 b}{12g}.$$

The stiffness K_l' of the leaf joint is defined when straight stiffness occurs as

$$K_l' = \frac{Eib}{g}.$$

The stiffness K_{m1} of the leaf joint is computed at the mass position m_1 results in linear stiffness by

$$K_{m1} = \frac{Eib}{n}.$$

The amplification ratio of the lever-type amplification mechanism (AR) with mass m_0 and b being the width of the beam is calculated by

$$AR = C/C_1.$$

The overall kinetic energy of the mechanism, so-called a mechanical system, includes the kinetic energy of the masses m_0, m_1, m_2, m_3, m_4, and m_5.

The kinetic energy of the mass m_0 is determined as

$$T_{m_0} = \frac{1}{2} j_0 \dot{\varphi}_0^2 = \frac{1}{2}\frac{1}{3} m_0 c^2 \left(\frac{\dot{y}_0}{c}\right)^2 = \frac{1}{6} m_0 \left(\dot{y}_0\right)^2,$$

in which j_0 is the moment of inertia, φ_0 is the rotational angle/angular displacement, and y_0 is the output displacement of the block m_0.

$$j_0 = \frac{1}{3} m_0 \times c^2.$$

At that time, the angular displacement φ_0 is calculated as follows

$$\varphi_0 = \frac{y_0}{c}.$$

The kinetic energy of the block m_1 is defined by

$$T_{m_1} = \frac{1}{2} m_1 \left(AR \times \dot{y}_0\right)^2.$$

The kinetic energy of the block m_2 is computed as

$$T_{m_2} = 8\frac{1}{2} m_2 \left(AR \times \dot{y}_0\right)^2.$$

The kinetic energy of the block m_3 is calculated by

$$T_{m_3} = 2\frac{1}{2} m_3 \left(AR \times \dot{y}_0\right)^2.$$

The kinetic energy of the block m_4 is determined as

$$T_{m_4} = \frac{1}{2} m_4 \left(AR \times \dot{y}_0\right)^2.$$

In the kinetic energy of the block m_5, the four vertical leaf springs are moving translationally, while the four horizontal leaf springs are performing rotational motion. It is determined as follows

$$T_{m_5} = 4\frac{1}{2} m_5 \left(AR \times \dot{y}_0\right)^2 + 4\frac{1}{2} j_5 \left(AR\dot{\varphi}_5\right)^2,$$

in which j_5 is the moment of inertia of the 4 horizontal leaf springs, φ_5 is the rotational angle of the 4 horizontal leaf springs, and y_0 is the output displacement of the block m_5

$$\begin{aligned}
j_5 &= \frac{1}{3} m_5 \times g^2, \\
\varphi_5 &= \frac{y_0}{g}, \\
T_{m_5} &= 4\frac{1}{2} m_5 \left(AR \times \dot{y}_0\right)^2 + 2\frac{1}{3} m_5 g^2 \left(\frac{AR \times \dot{y}_0}{g}\right)^2, \\
T_{m_5} &= 4\frac{1}{2} m_5 \left(AR \times \dot{y}_0\right)^2 + \frac{2}{3} m_5 \left(AR \times \dot{y}_0\right)^2.
\end{aligned}$$

The total kinetic energy of the entire mechanical system is yielded as

$$T = \frac{1}{6} m_0 \dot{y}_0^2 + \left(\frac{1}{2} m_1 + 4m_2 + m_3 + \frac{1}{2} m_4 + 2m_5 + \frac{2}{3} m_5\right) \left(AR \times \dot{y}_0\right)^2.$$

The equivalent K_{eq} hardness for the entire system is determined by

$$\frac{1}{K_{eq}} = \left(\frac{1}{K_{m1}} + 12\frac{1}{K_c} + \frac{1}{4K_l + 4K_l'}\right).$$

The potential energy for the whole mechanical system is calculated by

$$V = \frac{1}{2} K_{eq} y_0^2.$$

By using the Lagrange method, the dynamic equation* for the generalized coordinates y_i has the form as

$$\frac{\mathrm{d}}{\mathrm{d}t}\left(\frac{\partial L}{\partial \dot{y}_0}\right) - \frac{\partial L}{\partial \dot{y}_0} = 0,$$

where

$$L = T - V.$$

The equation* governing the free vibration of the system can be expressed as

$$M\ddot{Y} + KY = 0.$$

The equivalent mass M is calculated as

$$M = \frac{1}{3} m_0 + \left(2\left(\frac{1}{2} m_1 + 4m_2 + m_3 + \frac{1}{2} m_4 + \frac{8}{3} m_5\right)\right)(AR)^2.$$

The equivalent stiffness is determined as

$$K_{eq} = \frac{1}{\left(\frac{1}{K_{m1}} + 12\frac{1}{K_c} + \frac{1}{4K_l + 4K_l'}\right)}.$$

The first natural frequency of the designed mechanism is yielded as

$$f = \frac{1}{2\pi}\left(\frac{K_{eq}}{M}\right)^{0.5}. \tag{1}$$

From Eq. (1), the value of frequency is calculated as f = 50.34 Hz.

3.2. Finite element analysis

3.2.1. *Design of 3D model*

To perform the optimization tasks, a 3D model of a 1-DOF compliant mechanism is constructed in the geometry environment of ANSYS 2019R2 software. The proposed mechanism is designed in the form of a cantilever beam, and various types of joints, including right circular hinges and leaf joints, as shown in Fig. 5. The sixteen components of the 1-DOF mechanism are shown in Fig. 5, and the material parameters of PLA, are given in Table 2.

As depicted in Fig. 5, the designed mechanism is motivated to move in the y-axis. The lever (2) is received a force from the piezoelectric actuator (15). The motion from the

lever amplifier is transferred to the flexure joints. Then, the elastic energies are stored in the flexure joints (1), (3) (4), the parallel guiding mechanism (6), and the series of joints (8). It is noted that the parallel guiding mechanism (6) is arranged in symmetric topology, and the series of right circular hinges are designed in symmetry as well. These help to generate a single motion for the central positioning table (7). The outcomes of the proposed mechanism consist of the displacement and the first natural frequency of the central positioning table (7).

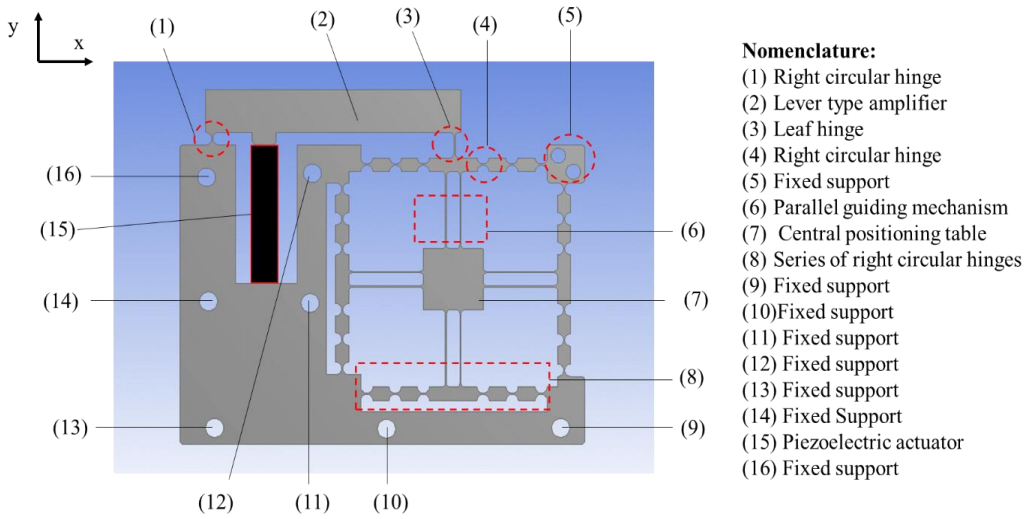

Fig. 5. 3D model of proposed 1-DOF compliant mechanism

In this study, the author selects the parameters of the spherical joints and the prismatic joints, specifically the types of joints in positions (1), (4), (6), and (8) as annotated in Fig. 5, as the optimization targets. This is because, in a 1-DOF mechanism, these joints experience the highest bending stress during motion, which significantly affects the mechanism's frequency. Therefore, the authors are chosen as the objectives for the further optimization problem.

3.2.2. *Meshing results*

The structure of the designed mechanism (Fig. 5) is operated based on the flexibility of joints, so that rigid joints do not deform during movement. Therefore, only coarse meshing is required for the rigid links (e.g., levers, fixed supports). Meanwhile, the flexible joints, including right circular joints and leaf joints are deformed during operation. Therefore, necessitating is to create a finer meshing for 25 right circular joints and 8 leaf joints. The employed meshing method is self-adjusting using Tet10 elements, which is

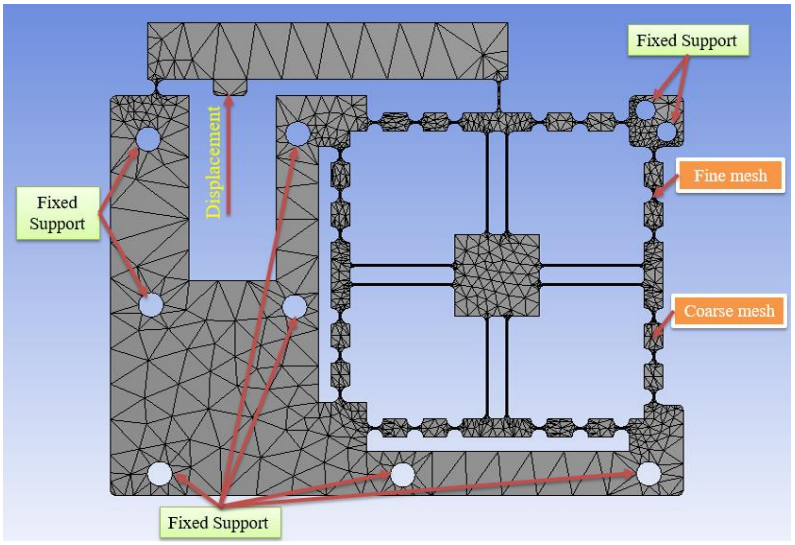

Fig. 6. Meshing results

the 10-node tetrahedral element, totaling 19406 elements and 40256 nodes to ensure convergence and accuracy of the analysis results. Meshing adheres to the Skewness standard [11], with a skewness result of 0.6. Boundary conditions and loads are illustrated as in Fig. 6. Convergence and distribution diagrams of mesh quality are based on the Skewness standard [12], as depicted in Fig. 7.

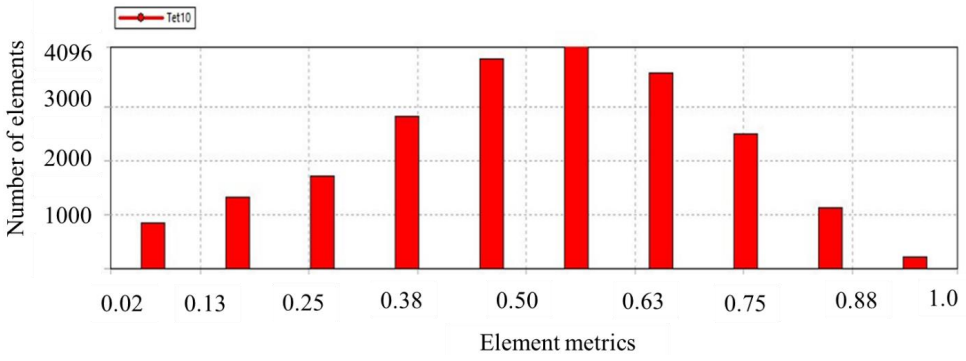

Fig. 7. The distribution diagram of mesh quality according to the Skewness standard

From Fig. 7, the results revealed that the skewness value reaches 0.6, and according to the previous research reference [12], the skewness values within the range of 0.5 to 0.6 ensure grid quality. Therefore, the grid partitioning results in this study achieving a value of 0.6, indicating a good mesh quality.

3.2.3. *Analysis of amplification ratio*

The central positioning table (mass m_4) can move in both X and Y directions. The main purpose of this paper is to design a mechanism which is moved in a single direction (Y-axis). The degrees of freedom are defined by the number of input actuators. As shown in Fig. 1 and Fig. 5, the input force along the Y-axis is given from a piezoelectric actuator. As a result, the central table m_4 will be moved in a Y direction and it is also be moved in the X direction. The movement in the Y-axis is the main motion of the proposed mechanism. Meanwhile, the movement in the X direction is a sub-movement, so-called parasitic motion error. The parasitic motion error in the X-axis will eliminate the positioning accuracy of the proposed mechanism. Hence, a parallel guiding mechanism is integrated with the central table so as to decrease the parasitic motion error. So, the proposed structure has 1-DOF. Furthermore, the simulation results in Fig. 8 reveal that the central table m_4 moves in a single Y direction.

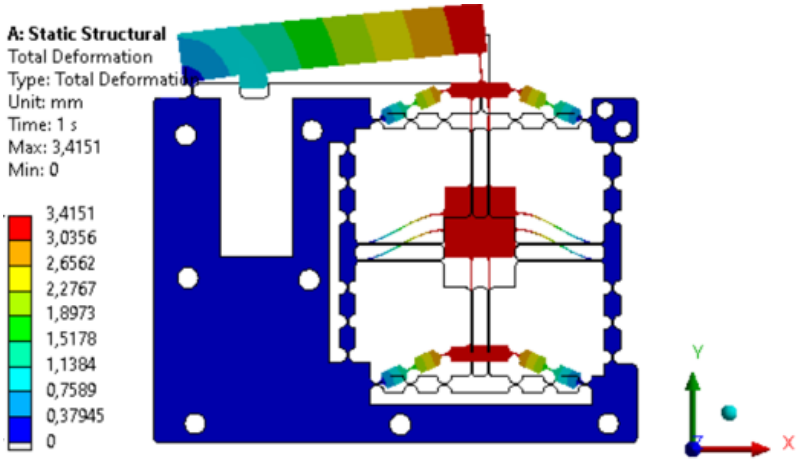

Fig. 8. Results of static simulation while the structure undergoes Y-movement

In this part, ANSYS Workbench 2019R2 software is utilized to assess the motion direction of the designed mechanism. Fig. 8 depicts the movement of the proposed mechanism only along the Y-axis. In this simulation, an input displacement of 1 mm is employed. The simulated displacement amplification ratio (DAR) is computed. The deviation error between the simulated DAR and the calculated DAR is about 7.8%, as given in Table 4.

In addition, the Y-direction output displacement of the central positioning table (mass m_4) is achieved about 3.41 mm, whereas the parasitic motion error in the X-direction is measured about 0.004 mm. Therefore, the coupling inaccuracy of the Y-axis with respect to the X-axis is calculated approximately 0.11%.

From Fig. 8 and the coupling inaccuracy of 0.11%, it can be concluded that the central positioning table is moved in the Y-axis with a small parasitic movement in the X-axis.

Table 4. Comparison between analytically derived values versus simulated values

Ratio of displacement amplification	Calculated value	FEM value	Deviation error
AR	3.69	3.41	7.8%

3.2.4. *Frequency verification*

Using ANSYS Workbench 2019R2 software, the Modal analysis system was employed to analyze the frequency of the proposed mechanism. Simulating the structure's frequency through the finite element analysis (FEA) method is yielded. The results found a preliminary frequency of 53.218 Hz before performing the computational optimization. The simulation results of the frequency through FEA are depicted in Fig. 9. The comparison error between the analytical method (Eq. (1)) and FEA results is about 5.4%, and the comparison results are presented in Table 5.

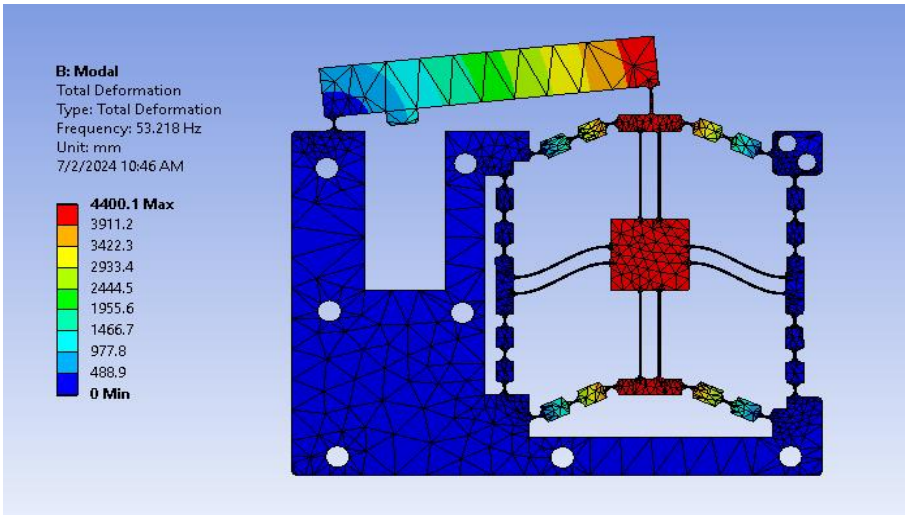

Fig. 9. Frequency simulation results

Table 5. The error between the calculated frequency and the simulated frequency

Frequency	Analytical calculation by Eq. (1)	FEA results	Error (%)
f (Hz)	50.34	53.218	5.4%

4. STRUCTURE OPTIMIZATION

4.1. Setup parametric factors

As illustrated in Figs. 5 and 6, the designed mechanism is operated based on the bending of a compliant joint [13]. Hence, the thickness dimension of the spherical compliant joints, the thickness dimension of the leaf spring joints, and the length of the leaf joint directly affect the mechanism's frequency. Therefore, in this mechanism, the frequency of the mechanism is set as the optimization target. The reason is that a high frequency can avoid a resonant phenomenon and can speed up the system. Accordingly, the thickness dimension of the right circular joint is denoted as j in the design model, corresponding to the value x_1 in the optimization problem. The thickness dimension of the leaf spring joint is denoted as i in the design model, corresponding to the value x_2 in the optimization problem, and the length dimension of the leaf joint is denoted as g in the design model, corresponding to the value x_3 in the optimization problem. Thus, the values x_1, x_2, x_3 are the variables to be optimized in the optimization problem. The symbols of the variables to be optimized are shown in Table 6.

Table 6. The geometric parameters of the flexure joints in the optimization problem

Variables	Definition	Unit	Variable value
j	Circular hinge thickness	mm	x_1
i	Leaf joint thickness	mm	x_2
g	Leaf joint length	mm	x_3

4.2. Setting up optimization environment

The frequency optimization process of the proposed mechanism comprises three main modules: (i) Geometric module, (ii) static analysis module, and (iii) optimization module. In the geometric module, the authors establish a model of the mechanism and identify the design variables such as input parameters. In the static analysis module, the material parameters of PLA are input, and the finite element analysis (FEA) simulations in ANSYS software are conducted to examine the initial frequency of the mechanism before optimizing. Thus, determining the constraints for the optimization problem are determined. In the optimization module, the design variables and the constraints regarding the frequency of the mechanism are added, and then the optimization process is carried out. The result of this process is an optimal solution for the frequency of the designed mechanism. The optimization flowchart of the 1-DOF mechanism is illustrated in Fig. 10.

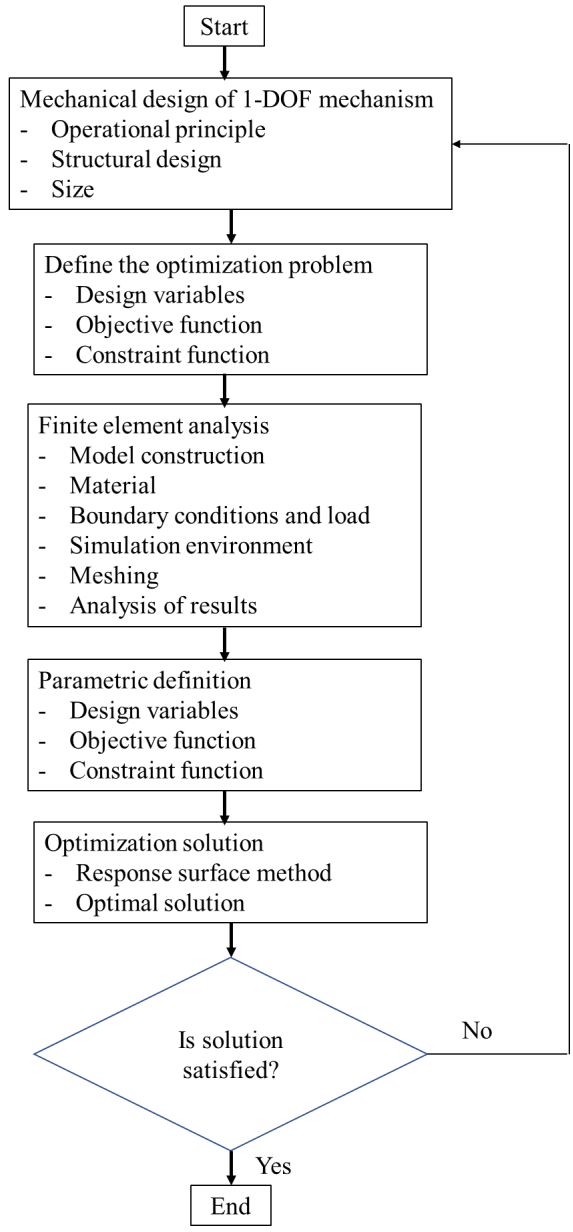

Fig. 10. Flowchart of the optimization problem for the 1-DOF mechanism

4.3. Setup ranges of design variables

In this study, the optimization problem is carried out with the goal of optimizing the frequency of the mechanism. The optimization problem is performed based on the principle of the water cycle algorithm. The principles of the water cycle algorithm are

presented in detail and can be found in the references [14, 15]. Thereby, increasing flexibility and reducing latency during operations.

Although the parallel guiding mechanism (6) guides the central table m_4 along the Y axis. However, during motion, the spring's stiffness is increased, so it effects to natural oscillation frequency. This could change the system's dynamic behavior. A greater natural frequency reduces the ability to absorb vibrations or oscillating forces from the environment, perhaps leading to stronger vibrations at higher frequencies. The leaf joint enhances the system's elasticity, which can increase effective stiffness (where deformation is minimal). As the stiffness is raised, the system's inherent frequency is also increased. Considering the series of joints (8) consists of 6 flexure joints (4), the six flexure joints (4) are particularly crucial since changing the thickness j (Fig. 1) has a considerable effect on the entire stiffness. When there is a circular joint, the spring elements' moment of inertia might influence the natural oscillation frequency. According to Eq. (1), the Lagrange equation indicates that as the stiffness K of the joints is increased, the natural frequency is raised accordingly. Therefore, the series flexure joints (6) and (8) in the optimization.

The optimization process is conducted through the following steps. First, because the 1-DOF structure is made by PLA material which can be printed using 3D printing technology [16, 17]. Therefore, the ranges of the parameters to be optimized, including x_1, x_2, x_3, are established as in Eqs. (2)–(6). Next, the authors proceed with the optimization process. The obtained results are given in Table 7. Subsequently, this process incorporates the constraint conditions $f(\mathbf{X})$ as in Eq. (6). Finally, after filtering the results, the best outcomes are shown in Table 8.

Find vector of design factor: $\mathbf{X} = [x_1, x_2, x_3]$

$$\text{Maximize} f(\mathbf{X}) : \tag{2}$$

Ranges of design factors

$$0.8 \text{ mm} \leq x_1 \leq 1.1 \text{ mm} \tag{3}$$

$$0.9 \text{ mm} \leq x_2 \leq 1.2 \text{ mm} \tag{4}$$

$$48 \text{ mm} \leq x_3 \leq 55 \text{ mm} \tag{5}$$

Subject to constraint

$$f(\mathbf{X}) > 53.218 \text{ Hz}. \tag{6}$$

Table 7. Design layout plan and computational results

No.	x_1 (mm)	x_2 (mm)	x_3 (mm)	$f(\mathbf{X})$ (Hz)
1	0.95	1.05	51.5	64.79
2	0.95	0.9	51.5	63.51

No.	x_1 (mm)	x_2 (mm)	x_3 (mm)	$f(\mathbf{X})$ (Hz)
3	0.95	1.2	51.5	66.909
4	0.8	1.05	51.5	54.398
5	1.1	1.05	51.5	74.616
6	0.95	1.05	48	64.291
7	0.95	1.05	55	66.682
8	0.82	0.92	48.65	55.237
9	0.82	1.17	48.65	60.028
10	1.072	0.92	48.654	70.311
11	1.072	1.172	48.6	75.238
12	0.82	0.92	54.34	55.738
13	0.82	1.172	54.34	55.792
14	1.07	0.92	54.346	71.44
15	7.07	1.17	54.3	76.548

Table 8. Optimal results

Optimal candidates	x_1 (mm)	x_2 (mm)	x_3 (mm)	$f(\mathbf{X})$ (Hz)
Candidates point 1	1.1	1.19	54.50	78.236
Candidates point 2	1.1	1.19	54.72	78.232
Candidates point 3	1.09	1.19	54.65	78.230

In Table 8, among three optimal candidates, the best solution is chosen as candidate #1 for the final design of the proposed mechanism because the first frequency is the highest.

4.4. Verification after optimization

To ensure the accuracy of the study, the author selected the best parameters from the optimization process (candidates #1). A new model of the 1-DOF mechanism is built, and then the authors proceed to simulate to check the verified frequency of the 1-DOF mechanism after the optimization process. The FEA results in Fig. 11 showed that the frequency of the 1-DOF mechanism after optimization is 75.927 Hz. The results indicated that the frequency of the mechanism after optimization is higher than the initial frequency (53.218 Hz), improving by 42.6%, as shown in Table 9.

Table 9. Comparison of frequency improvement after optimization

Frequency	Frequency before optimization	Frequency after optimization	Improvement (%)
f (Hz)	53.218	75.927	42.6

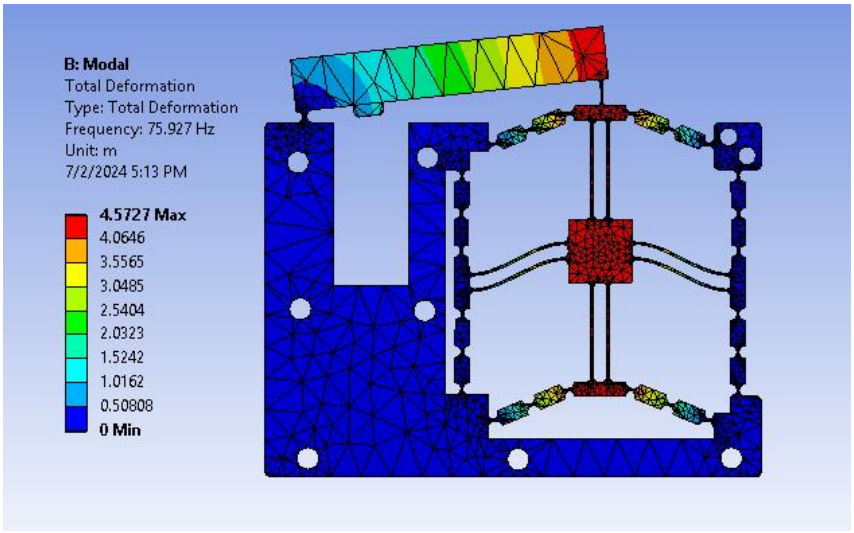

Fig. 11. Frequency verification of the optimized mechanism

4.5. Sensitivity analysis of the design variables

From the chart in Fig. 12, it can be seen that variable x_1 exhibits the most significant change. This variable represents the thickness of the right circular joint, indicating that changes in the thickness of the right circular joint will most significantly affect the frequency of the mechanism. On the other hand, variables x_2 and x_3 which represent the thickness of the leaf joint and the length of the leaf joint respectively, show that they have the least effect on the mechanism's frequency.

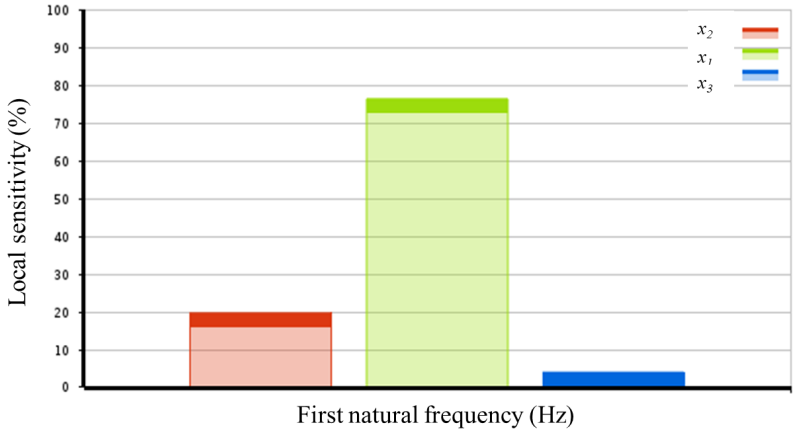

Fig. 12. The chart of the local sensitivity of the input parameters

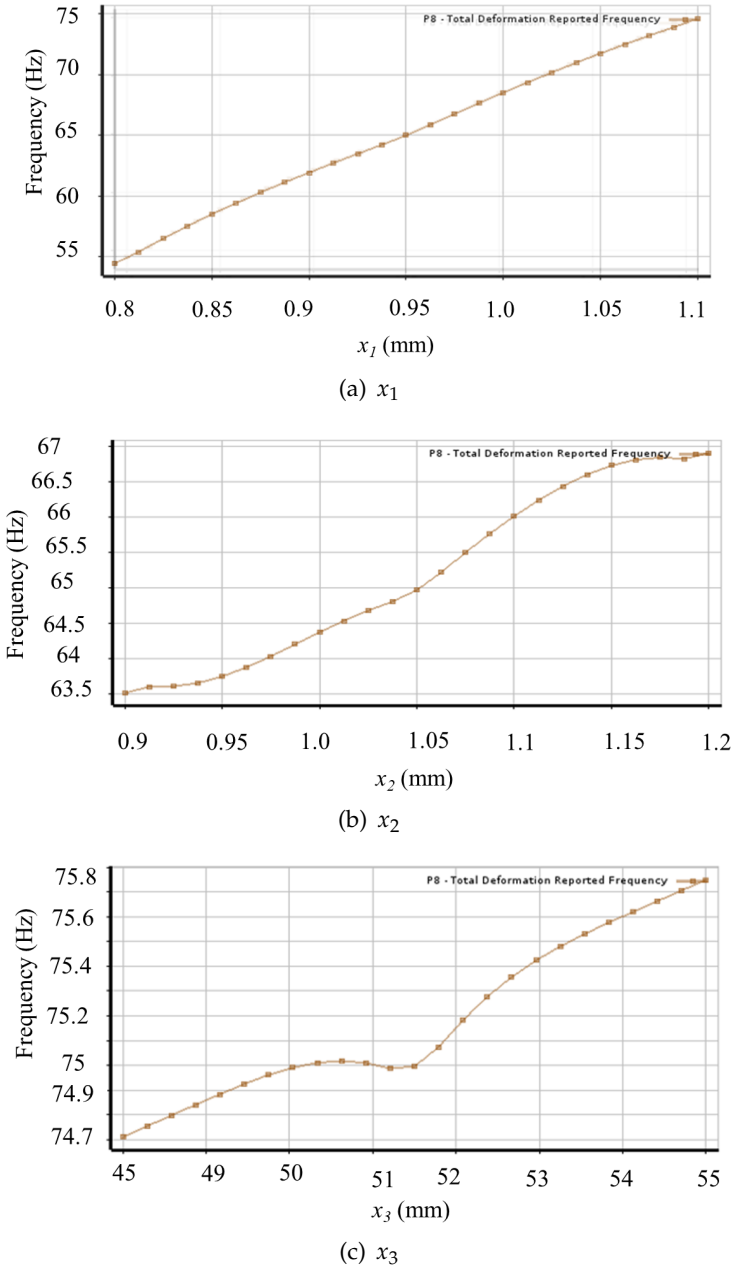

Fig. 13. Variable factors versus first natural frequency

Additionally, in Fig. 13(a), which represents the thickness of the ball joint, the linear chart remains unchanged, suggesting that this parameter has the greatest impact on the frequency. In contrast, Figs. 13(b) and 13(c), which represent the thickness of the leaf joint

and the length of the leaf joint, respectively, show nonlinear charts, indicating that these parameters have a smaller effect on the frequency compared to Fig. 13(a).

5. CONCLUSIONS

In this article, an optimization method for the first natural frequency of a 1-DOF compliant mechanism has been conducted. By employing the response surface methodology, the computational optimization has been presented. The main aim of this article was to enhance the first natural frequency of the mechanism, while reducing the size and efficiently utilizing materials. The result of the optimization process was a significant improvement in the frequency of the 1-DOF mechanism, increasing from 53.218 Hz to 75.927 Hz, achieving a percentage improvement in frequency of 42.6%. This accomplishment fulfilled the desired optimization target. The outcomes not only served as a theoretical basis for research but also opened avenues for practical applications in precision engineering systems. This optimization provided a better reference solution for real-world engineering applications and established a foundation for exploration and application in the future.

In upcoming studies, the experimentations on the real prototype by 3D printing technology. Physical experimentations are performing to verify the numerical results.

DECLARATION OF COMPETING INTEREST

The authors declare that they have no known competing financial interests or personal relationships that could have appeared to influence the work reported in this paper.

ACKNOWLEDGEMENT

This research was supported by the Ho Chi Minh City University of Technology and Education, project grant number B2023-SPK-03, funded by the Ministry of Education and Training, and hosted by the Ho Chi Minh City University of Technology and Education, Vietnam.

REFERENCES

[1] D. M. Ebenstein and L. A. Pruitt. Nanoindentation of biological materials. *Nano Today*, **1**, (2006), pp. 26–33. https://doi.org/10.1016/s1748-0132(06)70077-9.

[2] N. Alderete, A. Zaheri, and H. D. Espinosa. A novel in situ experiment to investigate wear mechanisms in biomaterials. *Experimental Mechanics*, **59**, (2019), pp. 659–667. https://doi.org/10.1007/s11340-019-00532-0.

[3] L. L. Howell, P. S. Magleby, and M. B. Olsen. *Handbook of compliant mechanisms*. Wiley, (2013). https://doi.org/10.1002/9781118516485.

[4] D. Stojiljković, M. Milošević, D. Ristić-Durrant, V. Nikolić, N. T. Pavlović, I. Ćirić, and N. Ivačko. Simulation, analysis, and experimentation of the compliant finger as a part of hand-compliant mechanism development. *Applied Sciences*, **13**, (2023). https://doi.org/10.3390/app13042490.

[5] J. D. Nowak, K. A. Rzepiejewska-Malyska, R. C. Major, O. L. Warren, and J. Michler. In-situ nanoindentation in the SEM. *Materials Today*, **12**, (2010), pp. 44–45. https://doi.org/10.1016/s1369-7021(10)70144-9.

[6] Z. Hu, K. J. Lynne, S. P. Markondapatnaikuni, and F. Delfanian. Material elastic–plastic property characterization by nanoindentation testing coupled with computer modeling. *Materials Science and Engineering: A*, **587**, (2013), pp. 268–282. https://doi.org/10.1016/j.msea.2013.08.071.

[7] L. Yuan, M. Ling, J. Lai, H. Li, and X. Zhang. Graphic transfer matrix method for kinetostatic and dynamic analyses of compliant mechanisms. *Journal of Mechanisms and Robotics*, **16**, (2023). https://doi.org/10.1115/1.4056827.

[8] N. L. Ho, M. P. Dang, and T.-P. Dao. Design and analysis of a displacement sensor-integrated compliant microgripper based on parallel structure. *Vietnam Journal of Mechanics*, (2020). https://doi.org/10.15625/0866-7136/14874.

[9] H. Peltola, E. Pääkkönen, P. Jetsu, and S. Heinemann. Wood based PLA and PP composites: Effect of fibre type and matrix polymer on fibre morphology, dispersion and composite properties. *Composites Part A: Applied Science and Manufacturing*, **61**, (2014), pp. 13–22. https://doi.org/10.1016/j.compositesa.2014.02.002.

[10] N. Graupner. Application of lignin as natural adhesion promoter in cotton fibre-reinforced poly(lactic acid) (PLA) composites. *Journal of Materials Science*, **43**, (2008), pp. 5222–5229. https://doi.org/10.1007/s10853-008-2762-3.

[11] N. L. Chau, H. G. Le, T.-P. Dao, and V. A. Dang. Design and optimization for a new compliant planar spring of upper limb assistive device using hybrid approach of RSM–FEM and MOGA. *Arabian Journal for Science and Engineering*, **44**, (2019), pp. 7441–7456. https://doi.org/10.1007/s13369-019-03795-w.

[12] N. L. Chau, H. G. Le, V. A. Dang, and T.-P. Dao. Development and optimization for a new planar spring using finite element method, deep feedforward neural networks, and water cycle algorithm. *Mathematical Problems in Engineering*, **2021**, (2021), pp. 1–25. https://doi.org/10.1155/2021/9921383.

[13] F. Dirksen and R. Lammering. On mechanical properties of planar flexure hinges of compliant mechanisms. *Mechanical Sciences*, **2**, (2011), pp. 109–117. https://doi.org/10.5194/ms-2-109-2011.

[14] A. Sadollah, H. Eskandar, A. Bahreininejad, and J. H. Kim. Water cycle algorithm with evaporation rate for solving constrained and unconstrained optimization problems. *Applied Soft Computing*, **30**, (2015), pp. 58–71. https://doi.org/10.1016/j.asoc.2015.01.050.

[15] M. Nasir, A. Sadollah, Y. H. Choi, and J. H. Kim. A comprehensive review on water cycle algorithm and its applications. *Neural Computing and Applications*, **32**, (2020), pp. 17433–17488. https://doi.org/10.1007/s00521-020-05112-1.

[16] P. Dudek. FDM 3D printing technology in manufacturing composite elements. *Archives of Metallurgy and Materials*, **58**, (2013), pp. 1415–1418. https://doi.org/10.2478/amm-2013-0186.

[17] V. Mazzanti, L. Malagutti, and F. Mollica. FDM 3D printing of polymers containing natural fillers: A review of their mechanical properties. *Polymers*, **11**, (2019). https://doi.org/10.3390/polym11071094.